



Fluctuations of the largest fragment charge in projectile fragmentation and its nonequilibrium effectJun Su ,* Long Zhu, and Erxi Xiao*Sino-French Institute of Nuclear Engineering and Technology, Sun Yat-sen University, Zhuhai 519082, China* (Received 6 July 2021; revised 19 October 2021; accepted 14 January 2022; published 16 February 2022)

Background: The projectile fragmentation is associated with the liquid-gas phase transition in the finite nuclear system. Recent experimental data and calculations by the statistical multifragmentation model indicated that the higher-order fluctuations of the largest fragment charge exhibit the signatures of the second-order phase transition [PLB809(2020)135763]. However, these higher-order fluctuations calculated by the dynamical model are still not reported.

Purpose: This work is proposed to investigate dynamically this signature and emphasize the nonequilibrium effect.

Methods: The isospin-dependent quantum molecular dynamics (IQMD) model is used to study the nonequilibrium thermalization and fragmentation in the $^{124}\text{Sn} + ^{120}\text{Sn}$ collisions at 600 MeV/nucleon. The minimum spanning tree algorithm is applied to distinguish the hot projectile-like system during the dynamics evolution.

Results: The fluctuations of the largest fragment charge Z_{max} up to the fourth order by the IQMD model reproduce the experimental data. The pseudocritical point indicated by zero of skewness (third-order fluctuation) together with minimum of kurtosis excess (fourth-order fluctuation) is found at impact parameter $b = 8.7$ fm, where the multifragmentation and nucleon evaporation are well balanced. Two observables are defined to describe the asymmetry of temperature and density in the projectile-like system. The nonequilibrium of the projectile-like system is verified by the distributions of these two observables. By comparing the distributions of the largest fragment charge for the equilibrium and nonequilibrium systems, it is found that the nonequilibrium of the hot projectile-like system influences the competitive relation between the multifragmentation and nucleon evaporation.

Conclusions: It is proposed that the nonequilibrium effect should be considered when study the pseudocritical point from the projectile fragmentation.

DOI: [10.1103/PhysRevC.105.024608](https://doi.org/10.1103/PhysRevC.105.024608)**I. INTRODUCTION**

A deeply investigated and universal phenomenon in statistical physics is the phase transition, which consists of changing symmetry characterized by a so-called order parameter within the smooth variation of an external driving parameter [1]. In nuclear physics, the liquid-gas phase transition is a natural phenomenon in infinite nuclear matter where the Van-der-Waals type of the nuclear force dominates [2–4]. It leads to a spinodal region defined by the negative isothermal compressibility, where the pure liquid phase is unstable and hence the system breaks into mix of the liquid and gas phases in equilibrium [5,6]. The multifragmentation in heavy-ion collisions at intermediate energies is proposed to observe the liquid-gas phase transition [7–14]. However, the conditions in finite hot nuclear system forming in the heavy-ion collisions are more complex comparing to that in the infinite system where the thermodynamic limit is satisfied. Although several signatures of the liquid-gas phase transition have been proposed but debates about the order of the phase transition and the critical properties still exist [15–20]. For instance, caloric

curve extracted using the isotopic thermometer displays a platform and suggests the first-order phase transition [21], but the platform is missing in the caloric curve extracted using the apparent temperatures [22].

Recent progresses associated with the phase transition in various different fields of physics are generalization and implementation in the nonequilibrium systems [23–26]. Indeed, the nonequilibrium effects are certainly important in heavy-ion collisions [8]. The nonequilibrium descriptions of the multifragmentation by nuclear transport models such as Boltzmann-Langevin type and quantum molecular dynamics type models have achieved success [6,27]. A comparison of phase transition signature measured in experiments with theoretical predictions by the event-by-event dynamics simulations looks rather significant.

It has been proposed that the higher-order fluctuations of the largest fragment size could provide a robust signature of the second-order phase transition [28]. Recent experimental data in the projectile fragmentation following $^{107,124}\text{Sn} + \text{Sn}$ and $^{124}\text{La} + \text{Sn}$ collisions at 600 MeV/nucleon and calculations by the statistical multifragmentation model (SMM) have supported this signature and further deduced pseudocritical point where two phases are well balanced [29]. However, these higher-order fluctuations calculated by the dynamical

*Corresponding author: sujun3@mail.sysu.edu.cn

model are still not reported. In our previous work, the data about the intermediate-mass fragments (IMFs) in $^{107,124}\text{Sn}$ and ^{124}La projectile fragmentation have been successfully reproduced with the isospin-dependent quantum molecular dynamics (IQMD) model [9]. The model has also been provided an uniform description of breakup mechanisms in the central collision, projectile fragmentation, and proton-induced spallation [6]. This work is proposed to investigate dynamically higher-order fluctuations of the largest fragment charge in projectile fragmentation and emphasize the nonequilibrium effect.

The paper is organized as follows. In Sec. II, the theoretical framework is described. In Sec. III, both the results and discussions are presented. Finally, Sec. IV presents conclusions.

II. THEORETICAL FRAMEWORK

In the IQMD model, the nucleons are represented by a Gaussian wave packet while the nuclear system is described by the N -body phase-space density. It is considered the time evolution of the nucleons under the mean field and the equivalent quantum jumps of the momenta performed by the binary nucleon-nucleon collisions with Pauli blocking. The version of the IQMD code used in this paper is IQMD-BNU (Beijing Normal University), which has been introduced and compared to other versions within the Transport Model Evaluation Project [30–32]. One can refer to the theoretical description of the model for projectile fragmentation in the Ref. [9]. Here we emphasize the improvement in several aspects.

First, the minimum spanning tree (MST) algorithm is applied to distinguish the hot system during the evolution. Nucleons with relative distance of coordinate and momentum of $|r_i - r_j| \leq 3.5$ fm and $|p_i - p_j| \leq 250$ MeV/ c belong to a hot system. The excitation energy per nucleon of the hot system can be calculated as follows:

$$E^* = \frac{\sum_i U_i + \sum_i \frac{(\mathbf{p}_i - \mathbf{p}_f)^2}{2m} - B(Z_f, A_f)}{A_f}. \quad (1)$$

Here U_i and \mathbf{p}_i are the single-particle potential and momentum of the i th nucleon; \mathbf{p}_f , Z_f , and A_f are the average momentum per nucleon, charge number, and mass number of the fragment; and $B(Z_f, A_f)$ is the binding energy of a nucleus with charge number Z_f and mass number A_f . The summation is for the nucleons belonging to the same hot system. The MST algorithm is performed at each time step, so that we can extract the properties of projectile spectator. Please refer to subsection A (“Properties of projectile spectator”) in Ref. [9] for details.

Second, to avoid the spurious emissions of nucleons and to preserve the number of prefragments, the evolution by the IQMD model will be stopped when the excitation energies of the two heaviest prefragments are less than a parameter E_{stop} . The parameter E_{stop} is determined from the onset of the multifragmentation as observed in heavy-ion reactions, about 3 MeV/nucleon [33]. In fact, this improvement of the IQMD model is the prominent contribution in Ref. [9]. It has been stated that there are spurious emissions of nucleons in the IQMD model due to the numerical fluctuations. It means

that a few nucleons will be evaporated even if one simulates a single nucleus in its ground state. As the time proceeds and for lighter nuclei, this effect becomes stronger. That is why the IQMD usually underestimates the multiplicity of the IMFs, which may disappear after spurious emissions of nucleons. If one can stop the dynamic simulation (by the IQMD model) and switch to the statistical simulation (by the GEMINI model) as soon as the process of the multifragmentation is over, then the spurious emissions will be controlled and the number of IMFs will be preserved. The MST algorithm and Eq. (1) make it possible. To be more specific, the fragments are distinguished and their excitation energies E^* are calculated and compared to E_{stop} at each time step during the dynamic evolution. When the condition $E^* < E_{\text{stop}}$ for the two heaviest prefragments is met, the dynamic evolution is stopped. In Ref. [9], we have proven that this improvement contributes to enhance the multiplicity of the IMFs.

Third, in order to describe the fermionic nature in the region where the binary collisions are scarce, the method of the phase-space density constraint (PSDC) [34] is applied. Noting that the common approach to consider the fermionic nature in the QMD type of models is the Pauli blocking in the nucleon-nucleon (NN) collisions. The binary NN collisions are allowed with the probability $(1 - f'_i)(1 - f'_j)$, in which f'_i and f'_j are the phase-space densities at the final states before the scattered particle is placed there. In the current work the PSDC method is used to better preserve the fermionic nature. The phase-space occupation probability \bar{f}_i is calculated by performing the integration on the hypercube of volume h^3 in the phase space centered around the i th nucleon at each time step,

$$\bar{f}_i = 0.621 + \sum_{j \neq i} \frac{\delta_{\tau_j, \tau_i}}{2} \int_{h^3} \frac{1}{\pi^3 \hbar^3} e^{-\frac{(r_j - r_i)^2}{2L} - \frac{(\mathbf{p}_j - \mathbf{p}_i)^2}{\hbar^2/2L}} d^3 r d^3 p, \quad (2)$$

where 0.621 is the contribution itself and τ_i represents isospin degree of freedom. At each time step and for each nucleon, the phase-space occupation \bar{f}_i is checked. If the phase-space occupation \bar{f}_i has a value greater than 1, the momentum of the i th nucleon is changed randomly by many-body elastic scattering. Meanwhile, the Pauli blocking in the binary NN collisions is modified. All the NN collisions for which the values of \bar{f}_i and \bar{f}_j are less than 1.0 are accepted [with a probability 1.0 rather than $(1 - f'_i)(1 - f'_j)$]. That is, by the many-body elastic scattering and the Pauli blocking in the binary NN collisions, the PSDC method ensures that \bar{f}_i and \bar{f}_j are always less than 1.0. It has been shown that the PSDC method is significant to describe the IMFs [6].

It is worth noting that the nuclear interaction applied in this work is momentum independent, see Eq. (4) in Ref. [9]. The momentum-dependent interaction (MDI) is optional in the IQMD-BNU model. It is important especially for studying the symmetry energy, see our previous works [35,36]. However, the MDI in the model inhibits the generation of the IMFs. The main reason is that the numerical approximation to solve the MDI lead to the spurious emission of nucleons. How to include the MDI in the IQMD model without numerical approximation is still an open question, and the next topic

in the Transport Model Evaluation Project. Before solve the problem, we often use the momentum independent interaction to study the observable about the IMFs. With this simplification, the stopping, radial flow, and other observable about the IMFs in the central collision, projectile fragmentation, and proton-induced spallation are reproduced quit well [6,8].

III. RESULTS AND DISCUSSIONS

A. Pseudocritical point indicated by higher-order fluctuations of the largest fragment charge

Useful measures of the fluctuations can be derived from the central moments. Both the dimensional and dimensionless cases are applied, see Refs. [37] and [29], respectively. Here we use the dimensionless cases, which are defined as

$$\begin{aligned} \mu_i &= \langle (Z_{\max} - \langle Z_{\max} \rangle)^i \rangle, & K_2 &= \frac{\mu_2}{\langle Z_{\max} \rangle^2}, \\ K_3 &= \frac{\mu_3}{\mu_2^{3/2}}, & K_4 &= \frac{\mu_4}{\mu_2^2} - 3, \end{aligned} \quad (3)$$

where Z_{\max} is the charge number of the largest fragment, $\langle \rangle$ denotes the ensemble average, K_2 is the variance normalized to the squared mean, K_3 is the skewness, and K_4 is the kurtosis excess. In order to illustrate the meaning of K_3 and K_4 , their values are calculated using the double Gaussian distribution,

$$\begin{aligned} N(Z_{\max}) \propto & (1-a) \exp \left[-\frac{(Z_{\max} - 20)^2}{5^2} \right] \\ & + a \exp \left[-\frac{(Z_{\max} - 40)^2}{5^2} \right]. \end{aligned} \quad (4)$$

As shown in Fig. 1, this double Gaussian distribution displays two peaks at $Z_{\max} = 20$ and 40 . The value of the parameter a indicates the proportions of two components. With increasing a , the proportion of the left peak decreases while the value of the skewness K_3 decreases. For the value $a = 0.5$ when two components are well balanced, the value of the skewness K_3 is close to zero and the kurtosis excess K_4 reaches its minimum. In the case of the second-order phase transition, the order parameter changes continuously as a function of the principal variable, indicating the transition of the states from an order to another. Due to the fluctuation, the order parameter for finite systems given principal variable distributes in a wide range, being similar to Eq. (4). The zero value of K_3 together with the minimum K_4 derived from the distribution of the order parameter provide a robust indication of the pseudocritical point, where two components with different orders are well balanced.

In the projectile fragmentation, the largest fragment charge (atomic number Z of the largest fragment) has been proved to be an order parameter to reveal the second-order phase transition [28,29]. We simulate the $^{124}\text{Sn} + ^{120}\text{Sn}$ collisions at 600 MeV/nucleon event-by-event by the IQMD model. The colliding systems producing same bound charge Z_{bound} are selected to calculate the fluctuations of the largest fragment charge Z_{\max} up to fourth order. In Fig. 2, the mean value $\langle Z_{\max} \rangle$, normalized variance K_2 , skewness K_3 , and kurtosis excess K_4 are shown as a function of Z_{bound} . In fact, those values have been extracted from the data in Ref. [29]. The

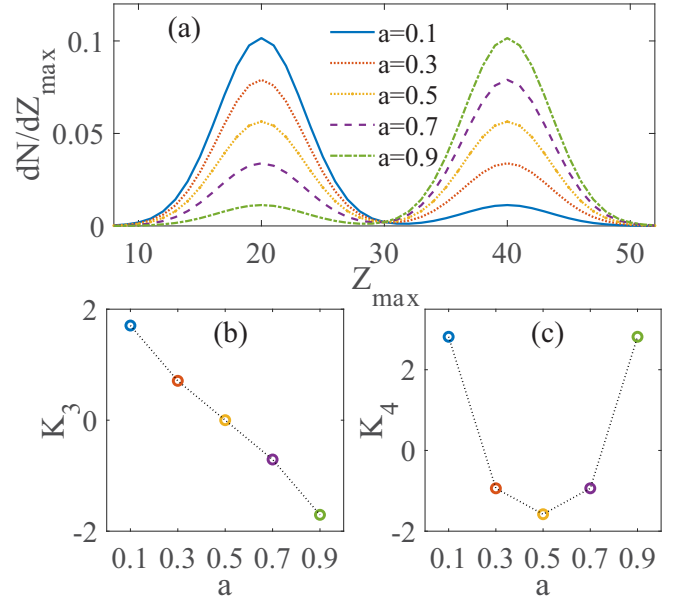


FIG. 1. (a) Double Gaussian distributions of the largest fragment charge with different bimodal ratios, the corresponding (b) skewness K_3 indicating the distribution asymmetry, and (c) the kurtosis excess K_4 measuring the degree of peakedness. The value $K_3 = 0$ and the minimum K_4 indicates the same proportion of two peaks.

figure shows that the calculations by the IQMD model agree with the data. With increasing Z_{bound} , the mean value of the largest fragment charge (Z_{\max}) increases, and the normalized

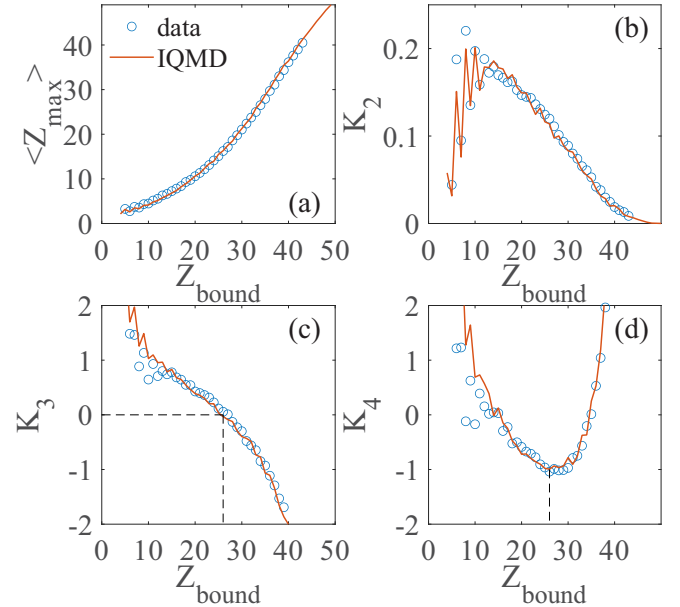


FIG. 2. Experimental data (circles) and calculations by the IQMD model (lines) of (a) the mean value $\langle Z_{\max} \rangle$ of the largest fragment charge, (b) the normalized variance K_2 , (c) the skewness K_3 , and (d) the kurtosis excess K_4 as a function of Z_{bound} in $^{124}\text{Sn} + ^{120}\text{Sn}$ collisions at 600 MeV/nucleon. Dashed curves indicate the pseudocritical point where $K_3 = 0$ and K_4 reaches the minimum.

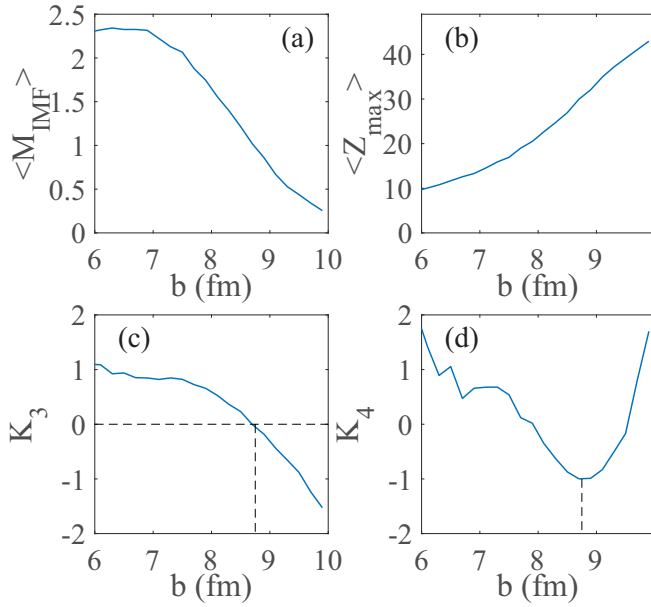


FIG. 3. (a) Mean multiplicity $\langle M_{\text{IMF}} \rangle$ of intermediate-mass fragments, (b) mean value $\langle Z_{\text{max}} \rangle$ of the largest fragment charge, (c) skewness K_3 , and (d) kurtosis excess K_4 as a function of the impact parameter b . Dashed curves indicate the pseudocritical point where $K_3 = 0$ and K_4 reaches the minimum.

variance K_2 displays an increasing tendency of oscillation for $Z_{\text{bound}} < 10$ then decreases for $Z_{\text{bound}} > 10$. The ensemble with $Z_{\text{bound}} = 27$ exhibits the zero transition of K_3 and the minimum of K_4 which indicates the pseudocritical point, shown as dashed curves in Figs. 2(c) and 2(d). It is one of the prominent results in Ref. [29].

The events are sorted using another principal variable, i.e., the impact parameter b , which cannot be measured directly in experiment or calculated by the statistical model. The impact parameter is an initial condition in the simulation by the dynamics model. The fluctuations as a function of the impact parameter provides a perspective on how the systems dissipate and fluctuate for a given initial condition. As shown in Fig. 3, $\langle Z_{\text{max}} \rangle$ vs b displays a tendency of monotonous increase, as like $\langle Z_{\text{max}} \rangle$ vs Z_{bound} . It is a natural result, since the bound charge of the fragments is monotonically correlated with the impact parameter. As is well known, the excited projectile-like systems decay mainly by the nucleon evaporation and multifragmentation. In the following, we will explain the competition between these two mechanisms and the corresponding fluctuation from the point of view of the energy dissipation. In midperipheral collisions (such as $b = 7.5$ fm), considerable incident energy dissipates into the thermal energy of the projectile-like system, leading to the multifragmentation. One sees a large value of the mean IMF multiplicity ($\langle M_{\text{IMF}} \rangle = 2.1$) for $b = 7.5$ fm in Fig. 3(a). With increasing impact parameter, the dissipated energy decreases and the decay mechanism of the hot projectile-like system changes from the multifragmentation to the nucleon evaporation. It is shown that the mean multiplicity of the IMF decreases to 0.2 at $b = 10$ fm. The nucleon evaporation and multifragmentation are nothing but

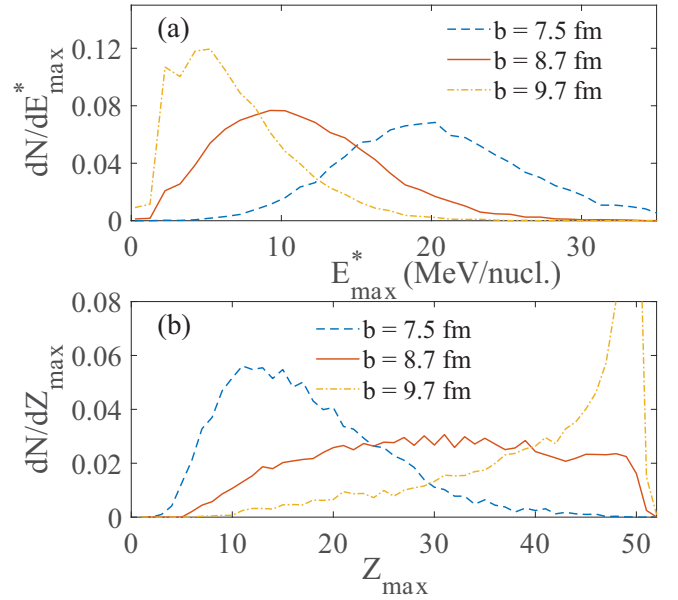


FIG. 4. Distributions of (a) maximum excitation energy of hot projectile-like system E^* and (b) largest fragment charge Z_{max} of the fragments in collision at $b = 7.5, 8.7,$ and 9.7 fm.

two kinds of orders in the decaying nuclear systems. In this case, the continuous change of $\langle M_{\text{IMF}} \rangle$ indicates the second-order phase transition. At $b = 8.7$ fm (shown as dashed curves in Fig. 3) and for $Z_{\text{bound}} = 27$ (shown as dashed curves in Fig. 2), two mechanisms are well balanced, so one sees the zero value of K_3 and the minima of K_4 .

During the evolution simulated by the IQMD model, the hot projectile-like system is distinguished by the MST algorithm together with the criterions of $Z < 50$ and $p_z > 0$, where Z is charge number and p_z is the momentum in the center-of-mass frame of the colliding system. The excitation energy of the hot projectile-like system is calculated and its maximum E^*_{max} during the evolution is a quantity to measure how many incident energies are dissipated. For collisions at $b = 7.5, 8.7,$ and 9.7 fm, the distributions of the maximum excitation energy E^*_{max} of the hot projectile-like system are shown in Fig. 4(a). With increasing impact parameter, the dissipated incident energy decreases, hence the most probable values of the excitation energy move left. As indicated by the fluctuation-dissipation theorem, more dissipation causes larger fluctuation. So one sees wider distribution at $b = 7.5$ fm than that at 9.7 fm. The distributions of the largest fragment charge Z_{max} are shown in Fig. 4(b). For collisions at $b = 7.5$ fm, the value of E^*_{max} distributes in a wide region along the center $E^*_{\text{max}} = 20$ MeV/nucleon, corresponding to the peak position $Z_{\text{max}} = 12$ and the long tail reaching $Z_{\text{max}} = 46$. With increasing impact parameter, the peak position of the E^*_{max} distribution moves left and that of the Z_{max} distribution moves right. For the case at $b = 9.7$ fm, the value of E^*_{max} distributes along 5 MeV/nucleon with a right-long tail, and that of Z_{max} distributes near $Z_{\text{max}} = 50$ and the left-long tail. At $b = 8.7$ fm, the wide distribution of Z_{max} from 10 to 50 is observed. Since the events at $b = 8.7$ fm provide

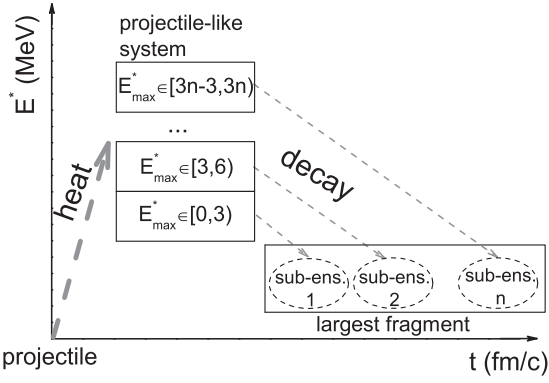


FIG. 5. Illustrating the heat and decay processes of the hot projectile-like system. The subensemble number n includes the events experiencing the states with excitation energy $E_{\max}^* \in [3n - 3, 3n)$.

$K_3 \simeq 0$ and minimum K_4 (see Fig. 3), it is called the well-balanced distribution. Difference between the ideal and real well-balanced distributions should be mentioned. The ideal case is the bimodal distribution, as shown in Fig. 1, but the real well-balanced distribution in the projectile fragmentation is unimodal and wide, as shown in Fig. 4(b).

In order to explain why the collisions at $b = 8.7$ fm cause the well-balanced distribution of Z_{\max} , the events are sorted by not only the impact parameter b but also another principal variable, i.e., the maximum excitation energy E_{\max}^* of the hot projectile-like system. As illustrated in Fig. 5, the projectile fragmentation consists of two processes, i.e., heating and decay. In the early state of the collision, the projectile is heated via the friction between the projectile and the target, resulting in a hot projectile-like system with excitation energy E_{\max}^* . Then the system decay by the nucleon evaporation or multifragmentation, producing the largest fragment (together with other IMF fragments and free nucleons). The ensemble including the collision events at $b = 8.7$ fm is divided into several subensembles. The subensemble number n includes the events in which the projectile-like systems are heated to the states with excitation energy $E_{\max}^* \in [3n - 3, 3n)$, where n is a positive integer. The Z_{\max} distributions in the subensembles 1 to 8 are shown in Fig. 6.

It is worth noting that the simulations of the IQMD model are stopped when the excitation energy of the heaviest prefragment is less than the threshold energy of the multifragmentation, i.e., 3 MeV/nucleon. The largest fragments in the subensemble 1 [Fig. 6(a)] are the projectile-like systems after heating. They have the charge number near 50. Those in the subensemble 2 [Fig. 6(b)] experience the decay from excitation energies in the region [6,3) to 3 MeV/nucleon. Several nucleons emit during the decay and the Z_{\max} distribution of the residual fragments become wider comparing to that in the subensemble 1. If one only considers the nucleon evaporation in the decay, with increasing E_{\max}^* (i.e., increasing id number of subensembles), then the number of the emission nucleons increases and hence the fluctuation of residual charge number are stronger. However, the presence of another decay mechanism, i.e., multifragmentation, breaks this trend. The inlet

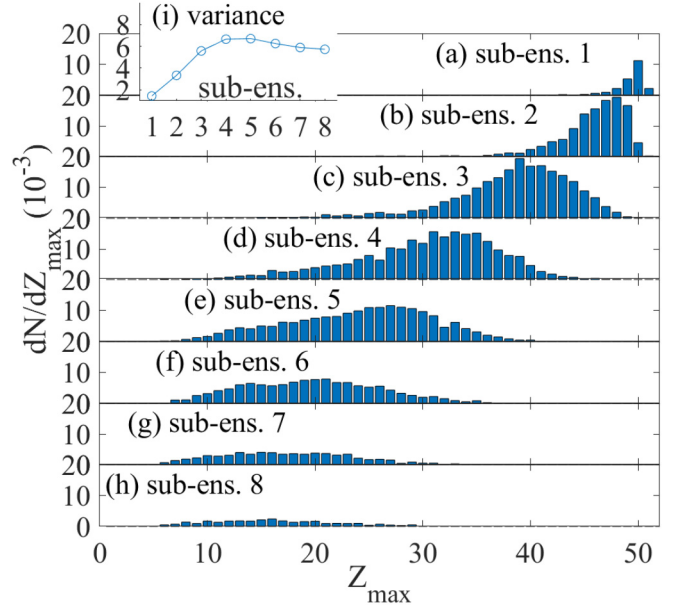


FIG. 6. Distributions of largest fragment charge Z_{\max} in the subensembles in collision at $b = 8.7$ fm. The definition of the subensembles is illustrated in Fig. 5. The inlet (i) displays the variances of the Z_{\max} distribution varies with the subensemble number.

(i) display the variances of the Z_{\max} distribution varies with the subensemble number. One sees in Fig. 6 that the widest Z_{\max} distribution occurs in subensembles 4 and 5 rather than subensembles with larger excitation energies.

B. Nonequilibrium effect

On the other hand, the nonequilibrium of the hot projectile-like system should be concerned in order to explain the fluctuation of the largest fragment charges. A necessary condition for equilibrium is an uniform temperature distribution. Linear fitting is carried out for the microscopic kinetic energies of nucleons as function of the coordinate in the x axis in the hot projectile-like system. The slope can be applied to measure if the temperature is uniform in the x axis,

$$L_x(E) = \frac{\sum_i^N x_i E_i - N \bar{x} \bar{E}}{\sum_i^N x_i^2 - N \bar{x}^2}, \quad (5)$$

where x_i and E_i are the coordinate in x axis and the kinetic energy in the center-of-mass frame of i th nucleon, \bar{x} and \bar{E} are their average values over the hot projectile-like system, and N is the number of the nucleons in the hot projectile-like system. A nonzero value of $L_x(E)$ means that the temperature is not uniform in the x axis. Replacing x by y (or z), one obtains the symmetry of the temperature in the y axis (or z axis). The symmetry of the density can be also defined by linear fitting for the density as function of the coordinate,

$$L_x(\rho) = \frac{\sum_i^N x_i \rho(\mathbf{r}_i) - N \bar{x} \cdot \bar{\rho}}{\sum_i^N x_i^2 - N \bar{x}^2}, \quad (6)$$

where \mathbf{r}_i is position of the i th nucleon and $\rho(\mathbf{r}_i)$ is the nucleon-density at position \mathbf{r}_i . Similarly, $L_y(\rho)$ and $L_z(\rho)$ are defined.

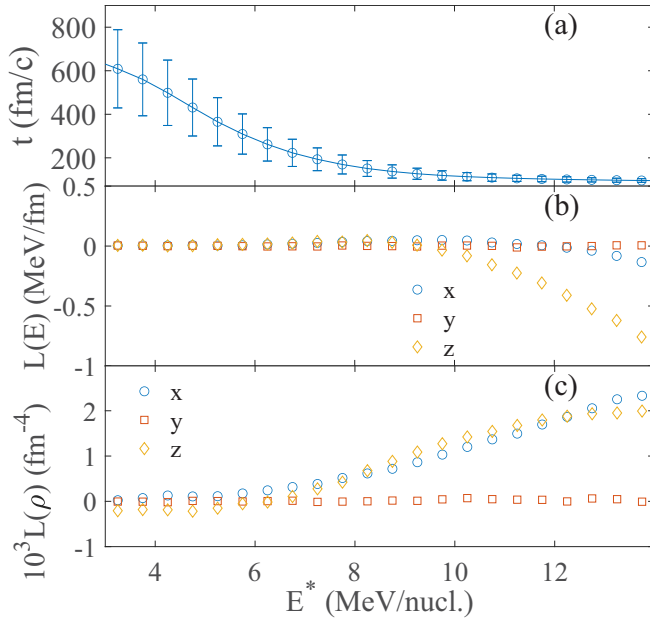


FIG. 7. (a) The evolution time to reach the excited state with the excitation energy E^* for the projectile-like system. The time $t = 0$ fm/c is chosen to be the moment when the distance between the projectile and the target is 70 fm. The error bar denotes the variance of the time distribution. Mean values of (b) $L(E)$ and (c) $L(\rho)$ as a function of the excitation energy E^* during the evolution.

A natural picture to study the dynamical evolution of a specific property is its time evolution. In fact, the time evolutions of several properties in the projectile fragmentation, such as density and isospin asymmetry, have been studied in our previous work [38]. With the help of the MST algorithm in the IQMD model, the excitation energy E^* of the hot projectile-like system as a function of the evolution time can be calculated. In the same way, the evolution-time to reach the excited state with the excitation energy E^* for the projectile-like system can also be extracted, as shown in Fig. 7(a). Here the time $t = 0$ fm/c is chosen to be the moment when the distance between the projectile and the target is 70 fm. The error bar denotes the variance of the time distribution. One sees that times to reach the excited states with $E^* > 10$ MeV/nucleon are almost the same. This time is nothing but the moment after the heating process. In the subsequent decay process, the fluctuation of the decay time is huge, although its mean value is monotonically correlated with the excitation energy. Comparing to the time evolution, property as a function of excitation energy E^* is better to study the evolution in the decay process.

The evolving states with the same excitation energy E^* are sorted to study the symmetry of the temperature and density along each axis in the rectangular coordinate system. The z axis is the direction of incidence of the projectile, and the x axis is the direction of the impact parameter. Values of $L(E)$ and $L(\rho)$ as a function of the excitation energy E^* are shown in Figs. 7(b) and 7(c). The initial symmetry in the y axis keeps during the collision, causing the values close to zero of $L_y(E)$ and $L_y(\rho)$. The asymmetry in the x and z axis are observed. The negative value of $L_x(E)$ at the excited state with $E^* = 14$

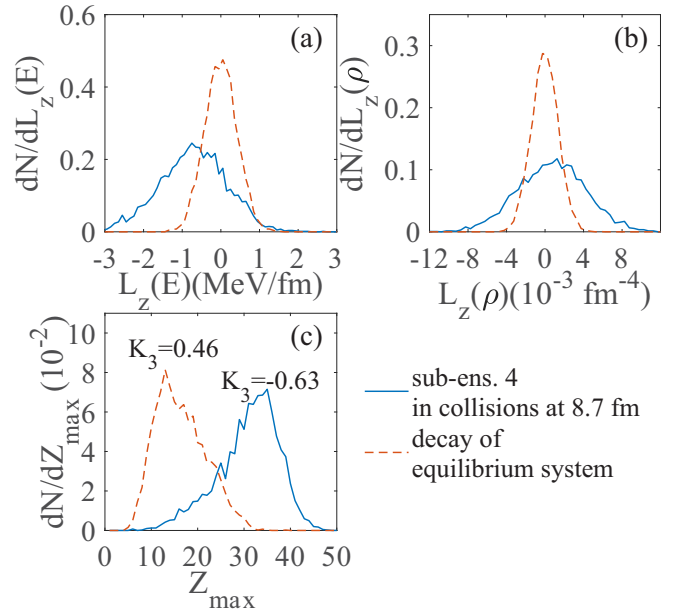


FIG. 8. Distributions of (a) $L_z(E)$, (b) $L_z(\rho)$, and (c) largest fragment charge Z_{max} in the subensemble 4 in the collisions at 8.7 fm and for the equilibrium systems with the excitation energies in the region from 9 to 12 MeV/nucleon.

MeV/nucleon indicates that the temperature of the projectile-like system in the side of friction is higher than the other side. However, this asymmetry is weak and transitory. The asymmetry of the temperature in the z axis is more obvious. The mean value of $L_z(E)$ is negative before the projectile-like system decay to the excited state with $E^* < 10$ MeV/nucleon. In the decay process, the projectile and target move far away from each other. The negative mean value of $L_z(E)$ indicates that the temperature of the projectile-like system in the participant side is higher. With the emission of the nucleons in the participant, E^* decreases and the projectile-like system returns to be symmetry. The positive values of $L_x(\rho)$ and $L_z(\rho)$ indicate smaller density in the friction and participant sides. The IMF should form mainly in these sides. This asymmetry keep until the projectile-like system decay to the states with $E^* < 6$ MeV/nucleon.

The symmetry mentioned above is an average over the ensemble. The distribution of $L_z(E)$ and $L_z(\rho)$ in the subensemble 4 are shown as solid curves in Figs. 8(a) and 8(b). One sees the wide distribution along $L_z(E) = 0.8$ MeV/fm and $L_z(\rho) = 1.5 \times 10^{-3}$ fm $^{-4}$. The nonzero centers indicate the nonequilibrium, and the wide distributions are caused by the fluctuation of the fine system. The nonequilibrium effect can be revealed by comparing the decays between the nonequilibrium system and the equilibrium system. The equilibrium systems with the excitation energies in the region from 9 to 12 MeV/nucleon, which is the same as those in the subensemble 4 in the collisions at 8.7 fm, are initialized in the IQMD model. The distribution of $L_z(E)$ and $L_z(\rho)$ in these equilibrium systems are shown as dashed curves in Figs. 8(a) and 8(b). Wide distributions are also seen, but the centers are zero. The decays of the equilibrium systems are simulated by the IQMD

model until the fragments with excitation energies less than 3 MeV/nucleon are formed. The distribution of largest fragment charge Z_{\max} in these productions are shown in Fig. 8(c) and comparing with that in the subensemble 4 in the collisions at 8.7 fm. The strong nonequilibrium effect can be found. For the equilibrium systems, the decay results in the asymmetric distribution along $Z_{\max} = 16$ with right tail. The skewness K_3 calculated from this distribution is 0.46. But in the collisions at 8.7 fm, the projectile is heated in one side, resulting in a nonequilibrium system. Figures 8(a) and 8(b) show that temperature in the heated side is higher and the density is smaller than those in the other side. Subsequently, the heat transfer is simultaneous with the decay. Local high temperature in the nonequilibrium system results in fast nucleon emission and suppress the multifragmentation. The corresponding distribution is along $Z_{\max} = 31$ with left tail. The skewness K_3 calculated from this distribution is -0.63 . $K_3 = 0.46$ for equilibrium systems and $K_3 = -0.63$ for nonequilibrium systems are in two sides of the pseudocritical point ($K_3 = 0.0$). Such a big difference indicates that the nonequilibrium effect should be considered when study the pseudocritical point from the projectile fragmentation.

We notice that the equilibrium hypothesis has been applied widely when studying the multifragmentation. For example, the authors in Ref. [29] assumed the equilibrium at some intermediate stage of the reaction and describe the experimental data well by the SMM model. The temperature T is an important input in the SMM model. However, the results in this work show that the fragmenting source forming in the heavy-ion collision is nonequilibrium, and also describe the experimental data well. It is indicated that the equilibrium system with the temperature T can decay in the same way as the nonequilibrium nuclear system forming in the heavy-ion collision. We define T as the equivalent temperature of the nonequilibrium nuclear system. Then an interesting question arises. Can one measure the equivalent temperature by the frequently used nuclear thermometer, such as the isotopic thermometer [39], the slope thermometer [40,41], and the kinetic thermometer [7]. This is the another story, which will be studied in our further work.

IV. CONCLUSION

Recent experimental data and calculations by the statistical multifragmentation model indicated that the higher-order fluctuations of the largest fragment charge exhibit the signature of a second-order phase transition [29]. This work is proposed to investigate this signature and emphasize the nonequilibrium effect. The $^{124}\text{Sn} + ^{120}\text{Sn}$ collisions at 600 MeV/nucleon are simulated by the IQMD model. The fluctuations of the largest fragment charge Z_{\max} up to fourth order are calculated. It is shown that the calculations of the fluctuations as a function of the total bound charge are quantitatively agree with the experimental data. Then the events are sorted using another principal variable, i.e., the impact parameter b , which cannot be measured directly in experiment or by the statistical model. The pseudocritical point indicated by zero of third-order fluctuation together with the minimum of fourth-order fluctuation are found in collisions at 8.7 fm, where the multifragmentation and nucleon evaporation are well balanced.

The minimum spanning tree algorithm is applied to distinguish the hot projectile-like system during the dynamics evolution. Two observables are defined to describe the asymmetry of temperature and density of the projectile-like system. One is the slope parameter in the linear fitting of microscopic kinetic energies of nucleons as function of their coordinate, and the other is the similar but replacing microscopic kinetic energies by the density. The nonequilibrium of the projectile-like system is verified by the distributions of these two observables. Since the projectile is heated in one side, the temperature in the heated side is higher and the density is smaller. This nonequilibrium influence the competitive relation between the multifragmentation and nucleon evaporation, which should be studied in detail when study the critical temperature from the projectile fragmentation.

ACKNOWLEDGMENTS

This work was supported by the National Natural Science Foundation of China under Grants No. 11875328 and No. 12075327.

-
- [1] L. D. Landau and E. M. Lifshitz, *Course of Theoretical Physics, Statistical Physics Part 1* (Elsevier, Amsterdam, 2013).
 - [2] K. Binder and D. P. Landau, *Phys. Rev. B* **30**, 1477 (1984).
 - [3] A. Guarnera, M. Colonna, and P. Chomaz, *Phys. Lett. B* **373**, 267 (1996).
 - [4] P. Chomaz, V. Dufloy, and F. Gulminelli, *Phys. Rev. Lett.* **85**, 3587 (2000).
 - [5] J. Su, L. Zhu, and C. Guo, *Phys. Lett. B* **782**, 682 (2018).
 - [6] J. Su, L. Zhu, C. Guo, and Z. Zhang, *Phys. Rev. C* **100**, 014602 (2019).
 - [7] J. Su, L. Zhu, W.-J. Xie, and F.-S. Zhang, *Phys. Rev. C* **85**, 017604 (2012).
 - [8] J. Su and F.-S. Zhang, *Phys. Rev. C* **87**, 017602 (2013).
 - [9] J. Su, W. Trautmann, L. Zhu, W.-J. Xie, and F.-S. Zhang, *Phys. Rev. C* **98**, 014610 (2018).
 - [10] F. Zhang, C. Li, P.-W. Wen, J.-W. Liu, J. Su, and F.-S. Zhang, *Phys. Rev. C* **100**, 024603 (2019).
 - [11] S. Sood, R. Kumar, A. Sharma, and R. K. Puri, *Phys. Rev. C* **99**, 054612 (2019).
 - [12] G. Chaudhuri and S. Mallik, *Phys. Rev. C* **99**, 054602 (2019).
 - [13] R. Wang, Y.-G. Ma, R. Wada, L.-W. Chen, W.-B. He, H.-L. Liu, and K.-J. Sun, *Phys. Rev. Research* **2**, 043202 (2020).
 - [14] Y. Huang, H. Zheng, R. Wada, X. Liu, W. Lin, G. Qu, M. Huang, P. Ren, J. Han, A. Bonasera *et al.*, *Phys. Rev. C* **103**, 014601 (2021).
 - [15] X. Campi, *Phys. Lett. B* **208**, 351 (1988).
 - [16] M. L. Gilkes, S. Albergo, F. Bieser, F. P. Brady, Z. Caccia, D. A. Cebra, A. D. Chacon, J. L. Chance, Y. Choi, S. Costa *et al.*, *Phys. Rev. Lett.* **73**, 1590 (1994).
 - [17] R. Botet, M. Płoszajczak, A. Chbihi, B. Borderie, D. Durand, and J. Frankland, *Phys. Rev. Lett.* **86**, 3514 (2001).

- [18] J. B. Elliott, L. G. Moretto, L. Phair, G. J. Wozniak, L. Beaulieu, H. Breuer, R. G. Korteling, K. Kwiatkowski, T. Lefort, L. Pienkowski *et al.*, *Phys. Rev. Lett.* **88**, 042701 (2002).
- [19] J. N. De, S. K. Samaddar, S. Shlomo, and J. B. Natowitz, *Phys. Rev. C* **73**, 034602 (2006).
- [20] E. Bonnet, D. Mercier, B. Borderie, F. Gulminelli, M. F. Rivet, B. Tamain, R. Bougault, A. Chbihi, R. Dayras, J. D. Frankland *et al.*, *Phys. Rev. Lett.* **103**, 072701 (2009).
- [21] J. Pochodzalla, T. Möhlenkamp, T. Rubehn, A. Schüttauf, A. Wörner, E. Zude, M. Begemann-Blaich, T. Blaich, H. Emling, A. Ferrero *et al.*, *Phys. Rev. Lett.* **75**, 1040 (1995).
- [22] Y.-G. Ma, A. Siwek, J. Péter, F. Gulminelli, R. Dayras, L. Nalpas, B. Tamain, E. Vient, G. Auger, C. O. Bacri *et al.*, *Phys. Lett. B* **390**, 41 (1997).
- [23] J. Steinheimer, J. Randrup, and V. Koch, *Phys. Rev. C* **89**, 034901 (2014).
- [24] G. Dagvadorj, J. M. Fellows, S. Matyjaśkiewicz, F. M. Marchetti, I. Carusotto, and M. H. Szymańska, *Phys. Rev. X* **5**, 041028 (2015).
- [25] F. Turci, C. P. Royall, and T. Speck, *Phys. Rev. X* **7**, 031028 (2017).
- [26] C. G. Wade, M. Marcuzzi, E. Levi, J. M. Kondo, I. Lestanovsky, C. S. Adams, and K. J. Weatherill, *Nat. Commun.* **9**, 1 (2018).
- [27] P. Napolitani and M. Colonna, *Phys. Rev. C* **92**, 034607 (2015).
- [28] J. Brzychczyk, *Phys. Rev. C* **73**, 024601 (2006).
- [29] T. Pietrzak, A. Botvina, J. Brzychczyk, N. Buyukcizmeci, A. Le Fèvre, J. Łukasik, P. Pawłowski, C. Sfienti, W. Trautmann, and A. Wieloch, *Phys. Lett. B* **809**, 135763 (2020).
- [30] J. Xu, L.-W. Chen, M. Y. B. Tsang, H. Wolter, Y.-X. Zhang, J. Aichelin, M. Colonna, D. Cozma, P. Danielewicz, Z.-Q. Feng *et al.*, *Phys. Rev. C* **93**, 044609 (2016).
- [31] Y.-X. Zhang, Y.-J. Wang, M. Colonna, P. Danielewicz, A. Ono, M. B. Tsang, H. Wolter, J. Xu, L.-W. Chen, D. Cozma *et al.*, *Phys. Rev. C* **97**, 034625 (2018).
- [32] A. Ono, J. Xu, M. Colonna, P. Danielewicz, C. M. Ko, M. B. Tsang, Y.-J. Wang, H. Wolter, Y.-X. Zhang, L.-W. Chen *et al.*, *Phys. Rev. C* **100**, 044617 (2019).
- [33] B. Borderie and M. Rivet, *Prog. Part. Nucl. Phys.* **61**, 551 (2008).
- [34] M. Papa, T. Maruyama, and A. Bonasera, *Phys. Rev. C* **64**, 024612 (2001).
- [35] J. Su, L. Zhu, C.-Y. Huang, W.-J. Xie, and F.-S. Zhang, *Phys. Rev. C* **94**, 034619 (2016).
- [36] J. Su, L. Zhu, C.-Y. Huang, W.-J. Xie, and F.-S. Zhang, *Phys. Rev. C* **96**, 024601 (2017).
- [37] R. V. Poberezhnyuk, O. Savchuk, M. I. Gorenstein, V. Vovchenko, K. Taradiy, V. V. Begun, L. Satarov, J. Steinheimer, and H. Stoecker, *Phys. Rev. C* **102**, 024908 (2020).
- [38] J. Su, L. Zhu, C. Guo, and F.-S. Zhang, *Chin. Phys. C* **44**, 084106 (2020).
- [39] S. Albergo, S. Costa, E. Costanzo, and A. Rubbino, *Nuovo Cimento A (1965-1970)* **89**, 1 (1985).
- [40] G. Westfall, B. Jacak, N. Anantaraman, M. Curtin, G. Crawley, C. Gelbke, B. Hasselquist, W. Lynch, D. Scott, B. Tsang *et al.*, *Phys. Lett. B* **116**, 118 (1982).
- [41] B. V. Jacak, G. D. Westfall, C. K. Gelbke, L. H. Harwood, W. G. Lynch, D. K. Scott, H. Stöcker, M. B. Tsang, and T. J. M. Symons, *Phys. Rev. Lett.* **51**, 1846 (1983).